
Rethinking Class-Discrimination Based CNN Channel Pruning

Yuchen Liu, David Wentzlaff, S.Y. Kung
Department of Electrical Engineering
Princeton University
{y116, wentzlaf, kung}@princeton.edu

Abstract

Channel pruning has received ever-increasing focus on network compression. In particular, class-discrimination based channel pruning has made major headway, as it fits seamlessly with the classification objective of CNNs and provides good explainability. Prior works singly propose and evaluate their discriminant functions, while further study on the effectiveness of the adopted metrics is absent. To this end, we initiate the first study on the effectiveness of a broad range of discriminant functions on channel pruning. Conventional single-variate binary-class statistics like Student's T-Test are also included in our study via an intuitive generalization. The winning metric of our study has a greater ability to select informative channels over other state-of-the-art methods, which is substantiated by our qualitative and quantitative analysis. Moreover, we develop a FLOP-normalized sensitivity analysis scheme to automate the structural pruning procedure. On CIFAR-10, CIFAR-100, and ILSVRC-2012 datasets, our pruned models achieve higher accuracy with less inference cost compared to state-of-the-art results. For example, on ILSVRC-2012, our 44.3% FLOPs-pruned ResNet-50 has only a 0.3% top-1 accuracy drop, which significantly outperforms the state of the art.

1 Introduction

Convolutional neural networks (CNNs) have become a mainstream machine learning model for various computer vision tasks, such as image classification [17, 46], image super resolution [31, 49], and semantic segmentation [38, 45]. To gain better prediction performance, a popular approach is to grow deeper and wider models. However, such CNNs require larger storage space and higher computational cost, making them unsuitable for edge devices like phones and embedded sensors.

Many methods have been proposed to reduce the storage space and inference latency of CNNs. For example: weight quantization [4, 5], tensor low-rank factorization [23, 28], weight-level pruning [14, 13, 15], and channel-level pruning [55, 20, 51, 27]. Among them all, channel-level pruning is the preferable method as it produces smaller dense models which can easily leverage high-efficiency Basic Linear Algebra Subprograms (BLAS) libraries [33].

Channel pruning has recently been fostered by the notion of evaluating the class-discriminative information with state-of-the-art works [55, 27]. Such methodology has two unique advantages: (1) It aims to find channels that have great linear separability with respect to the labels, which fits seamlessly with the goal of classification CNNs, to transform original distribution into a linearly separable space [16]. (2) It makes the pruning process more explainable, as it directly assesses what the channels have learned and quantitates the information of the channels in rigorous math. As illustrated in Figure 1, the channel with a low class-discriminative score has overlapped 2D projection and shows little class discrepancy visually. Such redundant channel is pruned away while the one with rich classification information is kept.

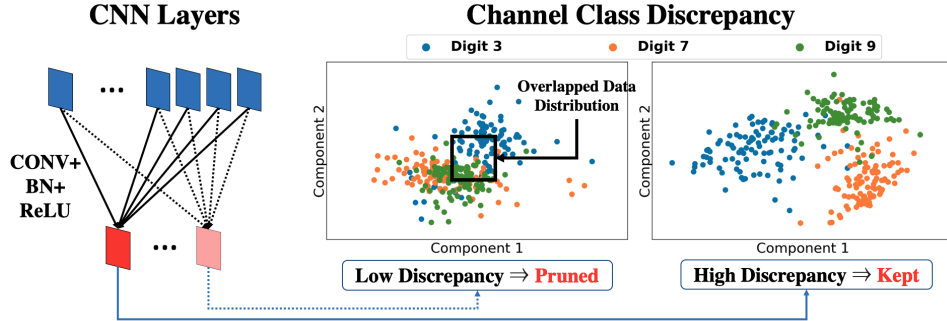


Figure 1: An illustration of discrimination-based channel pruning. Feature maps of two channels are picked from the second layer of LeNet-5 [30] fed with MNIST [29] input. The pruning decision is visually explainable, as shown in feature maps’ 2D projection. The channel with a low discrimination score (in dashed) is discarded as it has little class discrepancy. In contrast, the channel with a higher score displays clearer class separability and is kept during the pruning process. (Best viewed in color)

However, the effectiveness of the class-discriminative metrics in the prior works is not well studied. While [55] inserts a cross-entropy type loss and [27] uses a closed-form function, the metrics are proposed and evaluated singly without comparing to other existing well-defined discriminant functions, e.g., Maximum Mean Discrepancy (MMD) [11] on the channel pruning task. Moreover, well known single-variate binary-class statistics, like Student’s T-Test [32], are also mathematically defined to test the significance of two class’s difference, whilst no attempt has been made to generalize them for high-dimensional multi-label channel scoring. Moreover, current practices require iterative optimization steps or heavy matrix operation like matrix inversion to obtain the discrimination score, which can hinder the methods to be applied to larger networks and datasets.

We here have the first attempt to study the effectiveness over a variety of class-discriminative functions on channel pruning. The group of the interested functions includes not only high-dimensional metrics like the one proposed in [27] and MMD, but also several well-known single-variate binary-class statistics like Student’s T-Test [32], for which we initiate an intuitive and lightweight approach to generalize them for the high-dimensional multi-class channel scoring. Surprisingly, we find that one of our generalized single-variate metric, generalized Symmetric Divergence (G-SD), outperforms other functions notably, while having a relatively low computation complexity. Qualitative and quantitative analyses show that G-SD largely improves the selected channels’ quality over prior methods, including non-discriminative type metrics. In addition, we propose a FLOP-normalized sensitivity analysis scheme to evaluate the layer’s pruning sensitivity under the same FLOPs reduction. This scheme allows us to fairly compare layers’ redundancy across the model and automatically determine the pruning layers and number of pruning channels, which further enhances the pruning performance. We integrate G-SD and the FLOP-normalized sensitivity analysis into a unified pruning algorithm, via which we achieve state-of-the-art channel pruning results.

Our contributions are summarized as follows: (1) We conduct the first study on the effectiveness of a group of discriminant functions for channel pruning. The effectiveness of the winning metric, G-SD, is well explained by our qualitative and quantitative channel selection analysis, where it outperforms state-of-the-art methods with a clear margin. (2) We propose a FLOP-normalized sensitivity analysis for cross-layer pruning decision. We develop a pruning algorithm with the scheme and G-SD, which allows us to remove redundant channels without performance loss. (3) We demonstrate the advantages of our approach on three benchmark datasets (CIFAR-10, CIFAR-100, and ILSVRC-2012) with two widely used networks (VGGNet and ResNet). On ILSVRC-2012, our pruned ResNet-50 achieves 75.85% top-1 accuracy with 44.3% FLOPs reduction, surpassing the state of the art.

2 Related Work

Non-pruning Approaches. To reduce the computation complexity of CNNs, early works propose to factorize convolution kernels [23, 28, 53, 47]. Jaderberg et al. [23] explore a low-rank basis of filters to represent the full convolutional kernels, while Lebedev et al. [28] decompose a wide convolutional layer into a sequence of thinner layers. In addition, weight quantization methods are studied for CNN reduction [4, 5, 13, 44, 54]. Chen et al. [4] hash weights to different groups for storage saving.

Courbariaux et al. [5] and Rastegari et al. [44] binarize the network’s weights for inference speedup. Our methods can be applied directly upon these approaches to further accelerate the CNNs without specialized hardware/software.

Weight-level Pruning. Weight-level pruning aims to remove redundant weights, resulting in sparsely compressed networks [15, 14, 12, 48, 3, 52]. Han et al. [14] trim weights whose magnitudes are lower than a predefined threshold. Zhang et al. [52] adopt the alternating direction method of multipliers [2] for weight pruning. However, the produced sparse networks require specialized software libraries and hardware architectures to achieve the nominal acceleration.

Channel-level Pruning. In contrast, channel-level pruning can reduce network size and accelerate inference speed without specialized tools [33, 37, 39, 21, 40, 51, 22, 55, 20, 27, 50]. The core idea of channel pruning is to score the importance of channels and then drop the worthless ones. The channels’ importance can be assessed via their associated filters [33, 37, 39, 20, 18]. Li et al. [33] adopt ℓ_1 -norm of the filters as the pruning criterion. He et al. [20] calculate the filters’ geometric median and discard filters closest to it. Scoring channels’ saliency based on their activations is another popular direction [21, 40, 22, 51, 55, 27, 36]. He et al. [21] and Luo et al. [40] remove channels that have the least impact on the reconstructed mean square error. Yu et al. [51] propose neural importance score propagation (NISP) to score the channel importance in a more general manner.

In line with our work, several discrimination-based channel scoring methods have improved the efficacy of pruning [55, 27]. Zhuang et al. [55] insert discriminant losses to intermediate layers and prune channels that are less correlated to the losses after iterative steps. Kung et al. [27] achieve state-of-the-art pruning results by using a closed-form class-discriminative function, Discriminant Information (DI), for channel selection. While these studies solely focus on a single discriminant loss/metric, we provide more analysis on the effectiveness across a wide range of metrics, which is absent in the prior study. Moreover, we also pioneer to generalize conventional univariate binary-class statistics to serve for our channel importance evaluation. The winning metric in our study has much less time complexity comparing to the time-consuming loss optimization and DI’s heavy matrix inversion, while achieves a noticeable improvement upon them.

3 Methodology

3.1 Discriminant Function for Channel Pruning

Function Effectiveness Study. Although discriminant functions are all theoretically convincing, their empirical effectiveness on channel pruning remains understudied. To obtain more insights into their practical usefulness, we conduct a study over a group of discriminant functions. Our study includes high dimensional discrepancy metrics: Discriminant Information (DI) [27] and Maximum Mean Discrepancy (MMD) [11]. We also observe a group of conventional single-variate binary-class metrics which are well-defined for two-class discrimination measurement: Student’s T-Test (Ttest) [32], Absolute SNR (AbsSNR) [10], Symmetric Divergence (SD) [41], and Fisher Discriminant Ratio (FDR) [43]. We provide an intuitive approach to generalize them to high-dimensional multi-class channel scoring and name the generalized ones with a prefix ‘G-’ (G-Ttest, G-SD, .etc). Our implementation of these functions can be found in the Supplementary Material.

We study the empirical effectiveness of these functions by using them to conduct one-shot pruning for VGG-16 on CIFAR-10 and ResNet-38 on CIFAR-100, whose results are shown in Fig. 2. For each metric, we uniformly prune 10%, 20%, 30%, and 40% of channels with the lowest scores for all layers in both networks. These pruned models are then fine-tuned for 150 epochs by the SGD optimizer with Nesterov Momentum. All training hyper-parameters are the same for all metrics to allow a fair comparison. We evaluate the accuracies of the pruned models before and after the fine-tuning process, and include a random scoring method as the baseline. We find that the group of discriminant functions outperform the random baseline in nearly all pruning ratios, with and without fine-tuning. Moreover, we find a subset of leading metrics: G-SD, DI, and MMD, where G-SD has a clear improvement over the others. Without retraining, G-SD outperforms DI by 5.5% accuracy on CIFAR-10 with 40% channels removed and has an 8% accuracy gain on CIFAR-100 with 30% channels removed over MMD. With retraining, G-SD also performs the best among all other metrics on both tasks. For instance, it gains around 0.5% accuracy over MMD on CIFAR-100 when 30% channels removed. Based on such consistent winning results, we adopt G-SD as our channel selection criterion to conduct more class-discriminative pruning experiments.

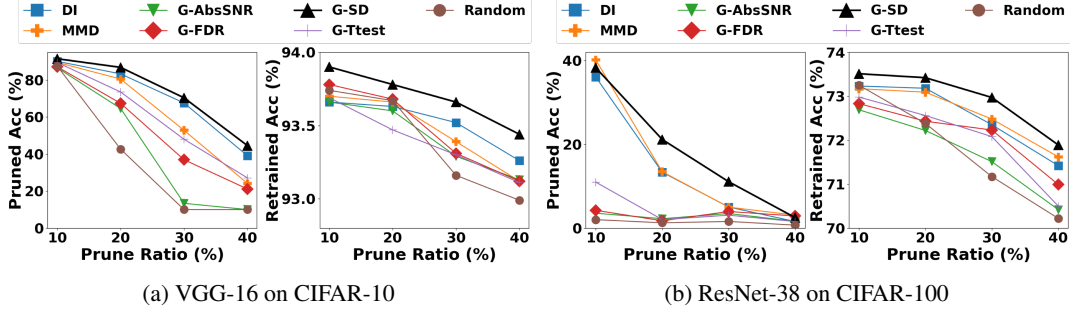


Figure 2: Function effectiveness study. The discriminant functions are applied to prune the networks with different layer pruning ratios. The pruned accuracies (without retraining) and retrained accuracies (with retraining) are plotted with respect to layer pruning ratios.

Winning Metric. Let us denote an n -sample 2-class single-variate dataset as $\mathcal{D} = \{(x_i, y_i)\}_{i=1}^n$, where $y_i \in \{0, 1\}$ is the class label associated with each sample $x_i \in \mathbb{R}$. Let $\mathcal{P} = \{x_i \mid (x_i, y_i) \in \mathcal{D}, y_i = 1\}$ and $\mathcal{Q} = \{x_i \mid (x_i, y_i) \in \mathcal{D}, y_i = 0\}$ denote two partitions of \mathcal{D} based on the labels, we can then formally define Symmetric Divergence (SD) [26] of \mathcal{D} as:

$$\text{SD}(\mathcal{P}, \mathcal{Q}) = \frac{1}{2} \left(\frac{\sigma_{\mathcal{P}}^2}{\sigma_{\mathcal{Q}}^2} + \frac{\sigma_{\mathcal{Q}}^2}{\sigma_{\mathcal{P}}^2} \right) + \frac{1}{2} \left(\frac{(\mu_{\mathcal{P}} - \mu_{\mathcal{Q}})^2}{\sigma_{\mathcal{P}}^2 + \sigma_{\mathcal{Q}}^2} \right) - 1 \quad (1)$$

where $\mu_{\mathcal{P}}$ and $\sigma_{\mathcal{P}}^2$ are the sample mean and sample variance of \mathcal{P} , and $\mu_{\mathcal{Q}}$ and $\sigma_{\mathcal{Q}}^2$ are the corresponding statistics of \mathcal{Q} .

SD is initially proposed to select discriminative individual features in bioinformatics feature vectors for dimension reduction and efficient classification [41]. The discriminant power of a single scalar feature is quantified by the first two terms of SD. The first term measures the *divergence* of two classes *symmetrically*. It achieves a high score for the feature whose $\sigma_{\mathcal{P}}^2$ or $\sigma_{\mathcal{Q}}^2$ is much smaller than the other, which indicates that one class of the feature has a more concentrated distribution, and thus the feature is more class distinguishable. The second term¹ awards features that have large ‘‘Signal-to-Noise Ratio (SNR)’’ [24] where the centroids distance $(\mu_{\mathcal{P}} - \mu_{\mathcal{Q}})^2$ can be viewed as ‘‘class discrimination signal’’ and the class variance sum $\sigma_{\mathcal{P}}^2 + \sigma_{\mathcal{Q}}^2$ is regarded as ‘‘class variational noise’’. Therefore, SD’s ability to find discriminant features is mathematically supported.

To generalize such function for the channel’s importance evaluation, the key is to find the corresponding statistics, $\mu_{\mathcal{P}}$, $\sigma_{\mathcal{P}}^2$, $\mu_{\mathcal{Q}}$, and $\sigma_{\mathcal{Q}}^2$ for the setting of channel scoring. To achieve this, we partition the feature maps of a channel in a one-versus-rest manner. We then apply a similar statistics operation on the partitioned high-dimensional tensor to obtain their corresponding $\mu_{\mathcal{P}}$, $\sigma_{\mathcal{P}}^2$, $\mu_{\mathcal{Q}}$, and $\sigma_{\mathcal{Q}}^2$. These statistics are then plugged back to Eqn. 1 to obtain the SD score for such partition. We finally aggregate the SD score for each partition to obtain a single scalar, G-SD score, which summarizes the channel’s importance. The details of such generalization can be found in Supplementary Material. The effectiveness of G-SD over state-of-the-art methods are further evidenced in our channel selection analyses shown in Fig. 3 and Fig. 4. G-SD incurs no expensive operations (e.g., matrix inversion, SVD), which makes it scalable to large networks and datasets.

3.2 FLOP-Normalized Sensitivity Analysis

Pruning Algorithm. For deep CNNs, layers are constructed heterogeneously as the number of FLOPs, the number of parameters, and the spatial size all vary across layers. Due to this, selecting pruning layers and determining number of pruning channels are crucial in the pruning procedure. A method to address the issue is to conduct the layer sensitivity analysis [33], where a two-step approach is proposed to quantitate a layer’s sensitivity: (1) remove a certain ratio of redundant channels from the layer; (2) evaluate the validation accuracy of the single-layer-pruned model without retraining. Such evaluation is repeated with different pruning ratios, and a pruning ratio vs. accuracy curve can be drawn for each layer to visualize the layer’s sensitivity. This inevitably makes the method

¹The expressions of SD’s second term vary a bit in [26] and [41]. In this work, we adopt the one in [26].

labor-intensive as the pruning layers and the number of pruned channels are decided via human analysis on each layer’s curve. Moreover, in step (1), removing the same ratio of channels in different layers could result in drastically different FLOPs reduction, which could make the analysis unfair.

To remedy these issues, we propose FLOP-normalized sensitivity analysis in Algorithm 1 to automate the structural pruning process with attention to the normalization of FLOP reduction. The effectiveness of our approach is shown in Fig. 5. Let us denote an L -layer model by \mathbf{M} , we aim to automatically determine the structure of the pruned model \mathbf{M}' . We denote a single-layer-pruned model by \mathbf{M}_ℓ^{-n} , which indicates that n channels are removed from layer l in \mathbf{M} . For each layer, we remove one single channel and calculate the resultant FLOPs reduction of the network by Eqn. 2. Such single-channel FLOPs loss at the l -th layer is denoted as FLOSS_ℓ .

$$\text{FLOSS}_\ell = \text{FLOP}(\mathbf{M}) - \text{FLOP}(\mathbf{M}_\ell^{-1}) \quad (2)$$

The number of pruning channels from layer l , n_l , can thus be determined in Eqn. 3, where $\text{FLOSS}_{\max} = \max_{\ell \in [1:L]} \text{FLOSS}_\ell$ and α is a scaling factor to control the pruning rate. Via the normalization of $\text{FLOSS}_{\max}/\text{FLOSS}_\ell$, removing n_l channels from layer l would have the same overall network’s FLOPs reduction. The derived n_l will be further rounded to integer.

$$n_\ell = \text{round}(\alpha \times \text{FLOSS}_{\max}/\text{FLOSS}_\ell) \quad (3)$$

We then follow the two-step analysis scheme: (1) individually prune n_l channels with the least G-SD from layer l to obtain $\mathbf{M}_\ell^{-n_\ell}$; (2) test the validation accuracy of $\mathbf{M}_\ell^{-n_\ell}$, Acc_l . Acc_l effectively quantifies layer l ’s sensitivity at the same FLOP’s reduction level. Finally, the pruned network \mathbf{M}' is obtained by choosing k layers with the highest Acc_l and pruned associated n_l channels from these layers. After structural pruning, \mathbf{M}' will be fine-tuned to recover the accuracy loss. By iterating this pruning-retraining process, we can obtain a compact model with high performance.

Algorithm 1: FLOP-Normalized Sensitivity Analysis

Input : Model \mathbf{M} , Number of Pruning Layers k
Output : Pruned Model \mathbf{M}'

- 1 Calculate FLOSS_ℓ by Eqn. 2
- 2 Calculate number of pruning channels n_l by Eqn. 3
- 3 **Evaluate Layer’s Sensitivity:** **for** $l \in [1 : L]$ **do**
- 4 Obtain $\mathbf{M}_\ell^{-n_\ell}$ by temporarily removing n_l channels in layer l
- 5 Test validation accuracy of $\mathbf{M}_\ell^{-n_\ell}$, Acc_l
- 6 **end**
- 7 Select layers with top- k Acc , $\{l_1, \dots, l_k\}$, and their number of pruning channels $\{n_1, \dots, n_k\}$
- 8 **Obtain Pruned Structure:** **for** $i \in [1 : k]$ **do**
- 9 Permanently prune n_i channels in layer l_i from \mathbf{M}
- 10 **end**
- 11 return \mathbf{M}'

Handling Skip Connection. For CNNs like ResNet, the input of a residual block is added to its output, which requires the number of channels to be the same for the block’s input and output. We adopt the idea of using a channel selection layer at the beginning of a residual block [21, 37]. Such layer samples a subset of input channels for the first convolution layer of the block based on their discriminative scores, which further reduces the block’s FLOPs and parameters without overheads.

4 Experimental Results

Benchmarks. We empirically evaluate our G-SD pruning method with VGGNet [46] and ResNet [17] on three image classification datasets, CIFAR-10 [25], CIFAR-100 [25], and ILSVRC-2012 [6]. CIFAR-10/100 contains 50K training samples and 10K test samples from 10/100 classes. ILSVRC-2012 contains 1.28M training images and 50K validation images in 1000 classes. We report pruned models at different FLOPs levels by adding a letter suffix (e.g., G-SD-A and G-SD-B). We compare G-SD pruning with previous approaches, e.g., ThiNet [40], DCP [55], GAL [36], FPGM [20], KSE [34], TAS [8], and DI [27]. Our method achieves state-of-the-art results on all benchmarks.

Training. Experiments are implemented in TensorFlow [1] and are carried out with NVIDIA Tesla P100 GPUs. We use the SGD optimizer with Nesterov Momentum [42] with a momentum of 0.9. The weight decay factor is set to 0.0001. We use the standard data augmentation scheme proposed in [17] for all datasets. On CIFAR, we fine-tune 200 epochs with a minibatch size of 128. The learning rate is initialized at 0.01 and divided by 5 at epoch 80 and 160. On ILSVRC-2012, we use a batch size of 256 to fine-tune VGG-16/ResNet-50 with 30/120 epochs. The learning rate is started at 0.0003 and multiplied by 0.4 at 40% and 80% of the total number of epochs. During the evaluation, the images are resized and center-cropped to the size of 224×224 .

(a) CIFAR-10 Dataset							
Network	Method	Test Acc. (%)	Acc. ↓ (%)	FLOPs	Pruned (%)	Parameters	Pruned (%)
VGG16	L1 [33]	93.25 → 93.40	-0.15	211M	34.2	5.40M	64.0
	GAL [36]	93.96 → 93.42	0.54	172M	45.2	2.67M	82.2
	SSS [22]	93.96 → 93.02	0.94	183M	39.6	3.93M	73.8
	G-SD	93.45 → 93.68	-0.23	62M	80.1	0.57M	96.2
ResNet 56	L1 [33]	93.04 → 93.06	-0.02	91M	27.6	730K	13.7
	GAL [36]	93.26 → 93.38	-0.12	78M	37.6	750K	11.8
	NISP [51]	93.04 → 93.01	0.03	71M	43.6	500K	42.6
	DCP [55]	93.80 → 93.49	0.31	63M	49.8	435K	49.2
	G-SD-A	93.40 → 93.95	-0.55	63M	49.6	510K	40.4
	TAS [8]	94.46 → 93.69	0.77	60M	52.7	-	-
	FPGM [20]	93.59 → 93.49	0.10	59M	52.6	-	-
	G-SD-B	93.40 → 93.84	-0.44	46M	63.0	407K	52.4
ResNet 110	L1 [33]	93.53 → 93.30	0.23	155M	38.6	1.18M	32.2
	NISP [51]	93.53 → 93.38	0.15	142M	43.8	0.99M	43.3
	G-SD-A	93.70 → 94.45	-0.75	136M	46.1	1.01M	41.6
	GAL [36]	93.50 → 92.74	0.76	130M	48.5	0.95M	44.8
	FPGM [20]	93.68 → 93.74	-0.06	121M	52.3	-	-
	G-SD-B	93.70 → 94.04	-0.34	101M	60.0	0.70M	59.4
(b) CIFAR-100 Dataset							
Network	Method	Test Acc. (%)	Acc. ↓ (%)	FLOPs	Pruned (%)	Parameters	Pruned (%)
VGG19	SLIM [37]	73.26 → 73.48	-0.22	256M	37.1	5.0M	75.1
	G-SD	73.40 → 73.67	-0.27	161M	59.5	3.2M	84.0
ResNet 164	LCCN [7]	75.67 → 75.26	0.41	197M	21.3	-	-
	SLIM [37]	76.63 → 76.09	0.54	124M	50.6	1.21M	29.7
	DI [27]	76.63 → 76.11	0.52	105M	58.0	0.95M	45.1
	G-SD	76.95 → 77.40	-0.45	92M	63.2	0.66M	61.8

Table 1: Experiments on CIFAR dataset. ‘-’: Results not reported in original papers.

Pruning. On CIFAR, all training data are feed-forwarded for G-SD channel scoring. On ILSVRC-2012, we randomly sample 10,000 training images for G-SD calculation in each pruning iteration. We choose k to be around one-third of the total number of layers and $\alpha \in [2, 4]$ for Algorithm 1.

4.1 CIFAR Experiments

We examine the performance of our scheme on CIFAR with five popular networks, VGG-16,19 and ResNet-56,110,164. We use the same VGGNet structures as [33, 37] with slim fully connected layers. As shown in Table 1, we achieve state-of-the-art results on both datasets for all networks.

On CIFAR-10, our VGG-16 has $5\times$ storage saving and $3\times$ inference speedup, while having 0.26% higher accuracy compared to GAL [36]. Our G-SD-A of ResNet-56 outperforms DCP [55] with 0.46% accuracy gain at the same FLOPs reduction ratio. Compared to FPGM [20] on ResNet-110, G-SD-B achieves 94.04% accuracy, which is 0.3% higher while having 8% less FLOPs. On CIFAR-100, our pruned VGG-19 has an accuracy gain of around 0.2% comparing to SLIM [37] with over 20% less FLOPs and around 10% fewer parameters. On ResNet-164, our pruned model outperforms DI [27] by 1.29% in accuracy with 5% less FLOPs and 16% fewer parameters. These results demonstrate that G-SD can produce more compact models with better performance compared to prior methods.

4.2 ILSVRC-2012 Experiments

We further conduct experiments on VGG-16 and ResNet-50 for large-scale ImageNet classification tasks. The results are summarized in Table 2 and we achieve state-of-the-art performance, again.

On VGG-16, our G-SD-A increases the performance in both top-1 and top-5 accuracy by 0.58% and 0.56% with $2.3\times$ acceleration from baseline. This result shows that the proposed metric has a strong regularization effect on deep CNNs, which helps remove deleterious nodes and improves generalization performance. Compared to FBS [9], our $3.3\times$ accelerated G-SD-B owns a higher speedup and compression ratio, while exceeds by 0.50% in top-5 accuracy. On ResNet-50, G-SD-A

Network	Method	Top-1 Acc. (%)	Top-1 ↓ (%)	Top-5 Acc. (%)	Top-5 ↓ (%)	FLOPs (B) Pruned (%)	Params (M) Pruned (%)
VGG16	L1 [33]	-	-	89.90 → 89.10	0.80	7.74 (50.0)	-
	CP [21]	-	-	89.90 → 89.90	0.00	7.74 (50.0)	-
	G-SD-A	71.30 → 71.88	-0.58	90.10 → 90.66	-0.56	6.62 (57.2)	133.61 (3.4)
	RNP [35]	-	-	89.90 → 86.67	3.23	5.16 (66.7)	138.34 (0.0)
	SLIM [37]	-	-	89.90 → 88.53	1.37	5.16 (66.7)	-
	FBS [9]	-	-	89.90 → 89.86	0.04	5.16 (66.7)	138.34 (0.0)
	G-SD-B	71.30 → 71.26	0.04	90.10 → 90.36	-0.26	4.68 (69.7)	131.19 (5.2)
ResNet 50	SSS [22]	76.12 → 74.18	1.94	92.86 → 91.91	0.95	2.82 (31.0)	-
	L1 [33]	76.12 → 72.88	3.24	92.86 → 91.05	1.81	3.07 (24.9)	-
	G-SD-A	76.15 → 76.21	-0.06	92.87 → 92.92	-0.05	2.90 (29.1)	21.91 (14.1)
	ThiNet [40]	72.88 → 72.04	0.84	91.14 → 90.67	0.47	2.44 (40.3)	16.94 (33.6)
	NISP [51]	72.88 → 71.99	0.89	-	-	2.29 (44.0)	14.36 (43.7)
	GAL [36]	76.15 → 71.95	4.20	92.87 → 90.94	1.97	2.33 (43.0)	21.20 (16.9)
	SFP [18]	76.15 → 74.61	1.54	92.87 → 92.06	0.81	2.38 (41.8)	-
	G-SD-B	76.15 → 75.85	0.30	92.87 → 92.66	0.21	2.28 (44.3)	19.59 (23.2)

Table 2: Experiments on ILSVRC-2012 dataset. ‘-’: Results not reported in original papers.

increases top-1 and top-5 accuracy both by around 0.05% at 30% of FLOPs reduction, which is rarely reported on ILSVRC-2012. As ResNet-50 has much less redundancy than VGG-16, such accuracy gain is even more promising. Moreover, G-SD-B achieves a 44.3% of FLOPs reduction with just 0.30% top-1 accuracy loss, which surpasses all previous methods. Compared to GAL [36], G-SD-B has a higher speedup ratio while achieves a nearly 4% top-1 accuracy gain from the same baseline.

5 Ablation Study

Our noticeable pruning performance is directly related to the use of G-SD and FLOP-normalized sensitivity analysis. We conduct the following ablation study to further illustrate their effectiveness in comparison with state-of-the-art methods.

5.1 Qualitative Channel Selection

Single Channel Visualization. We visualize the high G-SD and the low G-SD channels at the second layer of the first block in ResNet-50 with ILSVRC-2012 inputs. As shown in Col. 1-3 of Fig. 3, we observe that the channel with low G-SD value (**Col. 2**) tends to generate indistinguishable responses for different classes, while the high G-SD channel (**Col. 3**) well preserves the image patterns, which is more informative for classification. These suggest that G-SD is promising for channel selection.

Multiple Channels Visualization. To further visually compare the effectiveness of our G-SD with other channel selection criteria [33, 37, 20, 27], we score the channel activations and compute an average response over the top-10 channels with highest scores for each metric as shown in Col. 4-8 in Fig. 3. We observe that the average responses picked by G-SD (**Col. 8**) tends to display more class information than the ones from the other metrics (**Col. 4-7**). For example, in the first row, G-SD clearly separates the ostrich from the background grass, while others tend to generate mixed responses. Moreover, G-SD is the only one that preserves both the vertical nail and its long diagonal shadow in the fourth row. Such visual comparison speaks well on behalf of G-SD effectiveness.

5.2 Quantitative Channel Selection

We demonstrate the advantage of G-SD over state-of-the-art methods [33, 37, 27] quantitatively in Fig. 4, with VGG-16 on ILSVRC-2012 and ResNet-110 on CIFAR-10. Similar to the effectiveness study in 3.1, we use each metric to uniformly remove $r\%$ of the lowest-scored channels in all layers and include random scoring as the baseline. The accuracy of the pruned networks is evaluated without retraining to serve as the indicator of channels’ quality and the delegate of fine-tuned accuracy [14, 19]. r is set to be: 5, 10, 15, 20, 25, 30, 35, 40. We observe that G-SD wins against other methods in nearly all FLOPs reduction ratios on both networks and datasets. This analysis well explains G-SD’s effectiveness by comparing the selected channel’s quality directly and eliminating the effect of different retraining settings (optimizer, number of epochs, etc.) across literature.

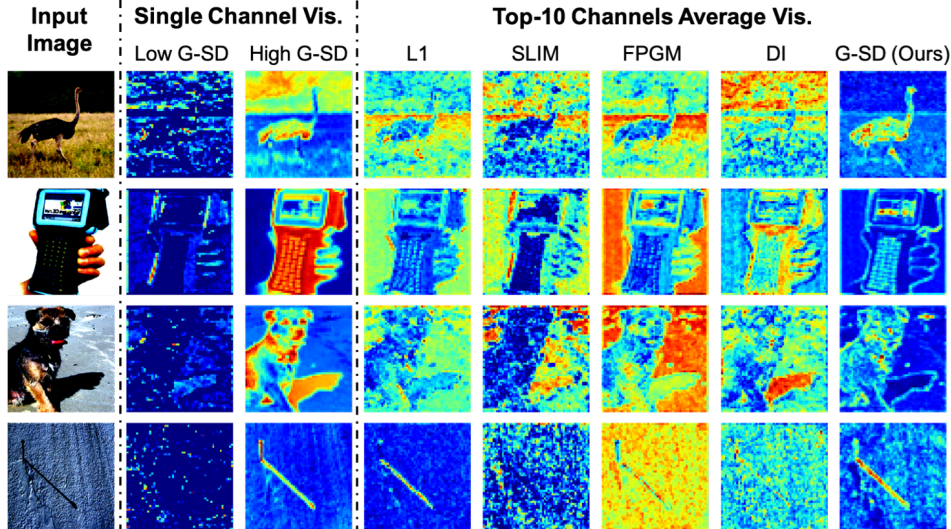


Figure 3: Qualitative channel selection analysis. **Col. 1:** Input images. **Col. 2-3:** Single channel visualization on channels with low and high G-SD values. **Col. 4-8:** Average responses of the top-10 channels selected by different metrics. From left to right, the metrics are: ℓ_1 -norm [33], batch-norm scaling factor [37], filter’s geometric median [20], DI [27], and G-SD.

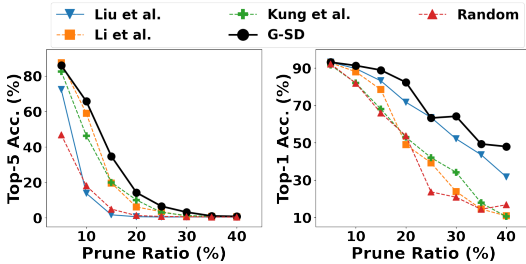


Figure 4: The curves of layer pruning ratio vs. accuracy (without retraining) with different channel scoring metrics. **Left:** VGG-16 on ILSVRC-2012. **Right:** ResNet-110 on CIFAR-10.

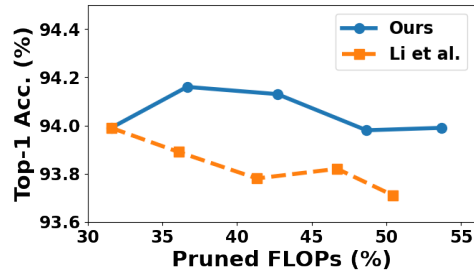


Figure 5: The curves of FLOPs pruning ratio vs. accuracy for two sensitivity analysis methods for ResNet-56 on CIFAR-10.

5.3 FLOP-Normalized Sensitivity Analysis

We compare our FLOP-normalized sensitivity analysis with the conventional sensitivity analysis proposed in [33] with ResNet-56 on CIFAR-10. Starting with a 31% FLOPs-pruned ResNet-56, we conduct five pruning-retraining iterations with G-SD by two methods. As shown in Fig. 5, we find a clear advantage for our methods over Li’s in every iteration. Moreover, the final network obtained by Li’s method suffers an accuracy drop of 0.3% while our model does not have accuracy loss.

6 Conclusion

In this paper, we conduct the first study on the empirical effectiveness of a broad range of class-discriminative functions in channel pruning. We provide an intuitive generalization to enable single-variate binary-class functions for channel scoring. We find that the winning metric in our study, generalized Symmetric Divergence (G-SD), selects channels with more information over prior arts via qualitative and quantitative analysis. In addition, we develop a FLOP-normalized sensitivity analysis scheme to enhance our pruning performance. Experimental results on three benchmark datasets demonstrate the advantage of our mechanism over state-of-the-art methods. In the future, we will explore the relationship between the channel’s class-discrimination and its redundancy in a more theoretical manner to help design better metrics.

References

- [1] Martín Abadi, Paul Barham, Jianmin Chen, Zhifeng Chen, Andy Davis, Jeffrey Dean, Matthieu Devin, Sanjay Ghemawat, Geoffrey Irving, Michael Isard, et al. Tensorflow: A system for large-scale machine learning. In *12th {USENIX} Symposium on Operating Systems Design and Implementation ({OSDI} 16)*, pages 265–283, 2016.
- [2] Stephen Boyd, Neal Parikh, Eric Chu, Borja Peleato, Jonathan Eckstein, et al. Distributed optimization and statistical learning via the alternating direction method of multipliers. *Foundations and Trends® in Machine learning*, 3(1):1–122, 2011.
- [3] Miguel A Carreira-Perpinán and Yerlan Idelbayev. “learning-compression” algorithms for neural net pruning. In *Proceedings of the IEEE Conference on Computer Vision and Pattern Recognition*, pages 8532–8541, 2018.
- [4] Wenlin Chen, James Wilson, Stephen Tyree, Kilian Weinberger, and Yixin Chen. Compressing neural networks with the hashing trick. In *International Conference on Machine Learning*, pages 2285–2294, 2015.
- [5] Matthieu Courbariaux, Itay Hubara, Daniel Soudry, Ran El-Yaniv, and Yoshua Bengio. Binarized neural networks: Training deep neural networks with weights and activations constrained to+ 1 or-1. *arXiv preprint arXiv:1602.02830*, 2016.
- [6] Jia Deng, Wei Dong, Richard Socher, Li-Jia Li, Kai Li, and Li Fei-Fei. Imagenet: A large-scale hierarchical image database. 2009.
- [7] Xuanyi Dong, Junshi Huang, Yi Yang, and Shuicheng Yan. More is less: A more complicated network with less inference complexity. In *Proceedings of the IEEE Conference on Computer Vision and Pattern Recognition*, pages 5840–5848, 2017.
- [8] Xuanyi Dong and Yi Yang. Network pruning via transformable architecture search. In *Advances in Neural Information Processing Systems*, pages 759–770, 2019.
- [9] Xitong Gao, Yiren Zhao, Lukasz Dudziak, Robert Mullins, and Cheng-zhong Xu. Dynamic channel pruning: Feature boosting and suppression. *arXiv preprint arXiv:1810.05331*, 2018.
- [10] Todd R Golub, Donna K Slonim, Pablo Tamayo, Christine Huard, Michelle Gaasenbeek, Jill P Mesirov, Hilary Coller, Mignon L Loh, James R Downing, Mark A Caligiuri, et al. Molecular classification of cancer: class discovery and class prediction by gene expression monitoring. *science*, 286(5439):531–537, 1999.
- [11] Arthur Gretton, Karsten M Borgwardt, Malte J Rasch, Bernhard Schölkopf, and Alexander Smola. A kernel two-sample test. *Journal of Machine Learning Research*, 13(Mar):723–773, 2012.
- [12] Yiwen Guo, Anbang Yao, and Yurong Chen. Dynamic network surgery for efficient dnns. In *Advances In Neural Information Processing Systems*, pages 1379–1387, 2016.
- [13] Song Han, Huizi Mao, and William J Dally. Deep compression: Compressing deep neural networks with pruning, trained quantization and huffman coding. *arXiv preprint arXiv:1510.00149*, 2015.
- [14] Song Han, Jeff Pool, John Tran, and William Dally. Learning both weights and connections for efficient neural network. In *Advances in neural information processing systems*, 2015.
- [15] Babak Hassibi and David G Stork. Second order derivatives for network pruning: Optimal brain surgeon. In *Advances in neural information processing systems*, pages 164–171, 1993.
- [16] Simon Haykin. *Neural networks: a comprehensive foundation*. Prentice Hall PTR, 1994.
- [17] Kaiming He, Xiangyu Zhang, Shaoqing Ren, and Jian Sun. Deep residual learning for image recognition. In *Proceedings of the IEEE conference on computer vision and pattern recognition*, pages 770–778, 2016.
- [18] Yang He, Guoliang Kang, Xuanyi Dong, Yanwei Fu, and Yi Yang. Soft filter pruning for accelerating deep convolutional neural networks. *arXiv preprint arXiv:1808.06866*, 2018.
- [19] Yihui He, Ji Lin, Zhijian Liu, Hanrui Wang, Li-Jia Li, and Song Han. Amc: Automl for model compression and acceleration on mobile devices. In *Proceedings of the European Conference on Computer Vision (ECCV)*, pages 784–800, 2018.
- [20] Yang He, Ping Liu, Ziwei Wang, Zhilan Hu, and Yi Yang. Filter pruning via geometric median for deep convolutional neural networks acceleration. In *Proceedings of the IEEE Conference on Computer Vision and Pattern Recognition*, pages 4340–4349, 2019.
- [21] Yihui He, Xiangyu Zhang, and Jian Sun. Channel pruning for accelerating very deep neural networks. In *Proceedings of the IEEE International Conference on Computer Vision*, pages 1389–1397, 2017.

- [22] Zehao Huang and Naiyan Wang. Data-driven sparse structure selection for deep neural networks. In *Proceedings of the European Conference on Computer Vision (ECCV)*, pages 304–320, 2018.
- [23] Max Jaderberg, Andrea Vedaldi, and Andrew Zisserman. Speeding up convolutional neural networks with low rank expansions. *arXiv preprint arXiv:1405.3866*, 2014.
- [24] Edwin T Jaynes. Information theory and statistical mechanics. *Physical review*, 106(4):620, 1957.
- [25] Alex Krizhevsky and Geoffrey Hinton. Learning multiple layers of features from tiny images. Technical report, Citeseer, 2009.
- [26] S.Y. Kung. *Kernel methods and machine learning*. Cambridge University Press, 2014.
- [27] S.Y. Kung, Zejiang Hou, and Yuchen Liu. Methodical design and trimming of deep learning networks: Enhancing external bp learning with internal omnipresent-supervision training paradigm. In *ICASSP 2019-2019 IEEE International Conference on Acoustics, Speech and Signal Processing (ICASSP)*, pages 8058–8062. IEEE, 2019.
- [28] Vadim Lebedev, Yaroslav Ganin, Maksim Rakhuba, Ivan Oseledets, and Victor Lempitsky. Speeding-up convolutional neural networks using fine-tuned cp-decomposition. *arXiv preprint arXiv:1412.6553*, 2014.
- [29] Yann LeCun. The mnist database of handwritten digits. <http://yann.lecun.com/exdb/mnist/>, 1998.
- [30] Yann LeCun, Léon Bottou, Yoshua Bengio, and Patrick Haffner. Gradient-based learning applied to document recognition. *Proceedings of the IEEE*, 86(11), 1998.
- [31] Christian Ledig, Lucas Theis, Ferenc Huszár, Jose Caballero, Andrew Cunningham, Alejandro Acosta, Andrew Aitken, Alykhan Tejani, Johannes Totz, Zehan Wang, et al. Photo-realistic single image super-resolution using a generative adversarial network. In *Proceedings of the IEEE conference on computer vision and pattern recognition*, pages 4681–4690, 2017.
- [32] Erich L Lehmann and Joseph P Romano. *Testing statistical hypotheses*. Springer Science & Business Media, 2006.
- [33] Hao Li, Asim Kadav, Igor Durdanovic, Hanan Samet, and Hans Peter Graf. Pruning filters for efficient convnets. *arXiv preprint arXiv:1608.08710*, 2016.
- [34] Yuchao Li, Shaohui Lin, Baochang Zhang, Jianzhuang Liu, David Doermann, Yongjian Wu, Feiyue Huang, and Rongrong Ji. Exploiting kernel sparsity and entropy for interpretable cnn compression. In *Proceedings of the IEEE Conference on Computer Vision and Pattern Recognition*, pages 2800–2809, 2019.
- [35] Ji Lin, Yongming Rao, Jiwen Lu, and Jie Zhou. Runtime neural pruning. In *Advances in Neural Information Processing Systems*, pages 2181–2191, 2017.
- [36] Shaohui Lin, Rongrong Ji, Chenqian Yan, Baochang Zhang, Liujuan Cao, Qixiang Ye, Feiyue Huang, and David Doermann. Towards optimal structured cnn pruning via generative adversarial learning. In *Proceedings of the IEEE Conference on Computer Vision and Pattern Recognition*, pages 2790–2799, 2019.
- [37] Zhuang Liu, Jianguo Li, Zhiqiang Shen, Gao Huang, Shoumeng Yan, and Changshui Zhang. Learning efficient convolutional networks through network slimming. In *Proceedings of the IEEE International Conference on Computer Vision*, pages 2736–2744, 2017.
- [38] Jonathan Long, Evan Shelhamer, and Trevor Darrell. Fully convolutional networks for semantic segmentation. In *Proceedings of the IEEE conference on computer vision and pattern recognition*, pages 3431–3440, 2015.
- [39] Christos Louizos, Max Welling, and Diederik P Kingma. Learning sparse neural networks through l_0 regularization. *arXiv preprint arXiv:1712.01312*, 2017.
- [40] Jian-Hao Luo, Jianxin Wu, and Weiyao Lin. Thinet: A filter level pruning method for deep neural network compression. In *Proceedings of the IEEE international conference on computer vision*, pages 5058–5066, 2017.
- [41] Man-Wai Mak and S.Y. Kung. A solution to the curse of dimensionality problem in pairwise scoring techniques. In *International Conference on Neural Information Processing*, pages 314–323. Springer, 2006.
- [42] Yurii E Nesterov. A method for solving the convex programming problem with convergence rate $o(1/k^2)$. In *Dokl. akad. nauk Sssr*, volume 269, pages 543–547, 1983.
- [43] Paul Pavlidis, Jason Weston, Jinsong Cai, and William Noble Grundy. Gene functional classification from heterogeneous data. In *Proceedings of the fifth annual international conference on Computational biology*, pages 249–255, 2001.

- [44] Mohammad Rastegari, Vicente Ordonez, Joseph Redmon, and Ali Farhadi. Xnor-net: Imagenet classification using binary convolutional neural networks. In *European Conference on Computer Vision*, pages 525–542. Springer, 2016.
- [45] Olaf Ronneberger, Philipp Fischer, and Thomas Brox. U-net: Convolutional networks for biomedical image segmentation. In *International Conference on Medical image computing and computer-assisted intervention*, pages 234–241. Springer, 2015.
- [46] Karen Simonyan and Andrew Zisserman. Very deep convolutional networks for large-scale image recognition. *arXiv preprint arXiv:1409.1556*, 2014.
- [47] Cheng Tai, Tong Xiao, Yi Zhang, Xiaogang Wang, et al. Convolutional neural networks with low-rank regularization. *arXiv preprint arXiv:1511.06067*, 2015.
- [48] Frederick Tung and Greg Mori. Clip-q: Deep network compression learning by in-parallel pruning-quantization. In *Proceedings of the IEEE Conference on Computer Vision and Pattern Recognition*, pages 7873–7882, 2018.
- [49] Xintao Wang, Ke Yu, Shixiang Wu, Jinjin Gu, Yihao Liu, Chao Dong, Yu Qiao, and Chen Change Loy. Esrgan: Enhanced super-resolution generative adversarial networks. In *Proceedings of the European Conference on Computer Vision (ECCV)*, pages 0–0, 2018.
- [50] Jianbo Ye, Xin Lu, Zhe Lin, and James Z Wang. Rethinking the smaller-norm-less-informative assumption in channel pruning of convolution layers. *arXiv preprint arXiv:1802.00124*, 2018.
- [51] Ruichi Yu, Ang Li, Chun-Fu Chen, Jui-Hsin Lai, Vlad I Morariu, Xintong Han, Mingfei Gao, Ching-Yung Lin, and Larry S Davis. Nisp: Pruning networks using neuron importance score propagation. In *Proceedings of the IEEE Conference on Computer Vision and Pattern Recognition*, pages 9194–9203, 2018.
- [52] Tianyun Zhang, Shaokai Ye, Kaiqi Zhang, Jian Tang, Wujie Wen, Makan Fardad, and Yanzhi Wang. A systematic dnn weight pruning framework using alternating direction method of multipliers. In *Proceedings of the European Conference on Computer Vision (ECCV)*, pages 184–199, 2018.
- [53] Xiangyu Zhang, Jianhua Zou, Xiang Ming, Kaiming He, and Jian Sun. Efficient and accurate approximations of nonlinear convolutional networks. In *Proceedings of the IEEE Conference on Computer Vision and pattern Recognition*, pages 1984–1992, 2015.
- [54] Shuchang Zhou, Yuxin Wu, Zekun Ni, Xinyu Zhou, He Wen, and Yuheng Zou. Dorefa-net: Training low bitwidth convolutional neural networks with low bitwidth gradients. *arXiv preprint arXiv:1606.06160*, 2016.
- [55] Zhuangwei Zhuang, Mingkui Tan, Bohan Zhuang, Jing Liu, Yong Guo, Qingyao Wu, Junzhou Huang, and Jinhui Zhu. Discrimination-aware channel pruning for deep neural networks. In *Advances in Neural Information Processing Systems*, pages 883–894, 2018.

Supplementary Materials

We organize our supplementary material as follows. In Section 7, we present the definitions of the studied discriminant functions (except SD) as well as the details of our generalization for single-variate binary-class functions to high-dimensional multi-class channel scoring. In Section 8, we discuss the detailed structures of the pruned VGG-16 and ResNet-50 models on ILSVRC-2012 by generalized Symmetric Divergence (G-SD). We discuss an empirical study on the time complexity of two discriminant functions, G-SD and Discriminant Information (DI) [27], for channel scoring in Section 9. In Section 10, we provide more visualizations of our qualitative channel selection analysis.

7 Discriminant Functions

7.1 Single-Variate Binary-Class Metrics

We adopt the same notation of the n -sample binary-class single-variate dataset as in the main paper. Our implementation of Absolute SNR (AbsSNR) [10], Fisher Discriminant Ratio (FDR) [43] and Student’s T-Test (Ttest) [32] are:

$$\text{AbsSNR}(\mathcal{P}, \mathcal{Q}) = \frac{|\mu_P - \mu_Q|}{\sigma_P + \sigma_Q} \quad (4)$$

$$\text{FDR}(\mathcal{P}, \mathcal{Q}) = \frac{(\mu_P - \mu_Q)^2}{\sigma_P^2 + \sigma_Q^2} \quad (5)$$

$$\text{Ttest}(\mathcal{P}, \mathcal{Q}) = \frac{|\mu_P - \mu_Q|}{\sqrt{\frac{\sigma_P^2}{|\mathcal{P}|} + \frac{\sigma_Q^2}{|\mathcal{Q}|}}} \quad (6)$$

where $|\mathcal{P}|$ and $|\mathcal{Q}|$ denote the number of samples in \mathcal{P} and \mathcal{Q} .

7.2 Generalization

We observe that the computation of these three metrics along with SD mainly requires four statistics: μ_P , σ_P^2 , μ_Q , and σ_Q^2 . We here use SD as an example to demonstrate our way to find these statistics for CNN’s channel scoring, while the other three metrics can follow the similar way.

Notation. For an N -sample C -class dataset, we denote the feature maps of a CNN channel as $\mathcal{F} = \{(f_i, c_i)\}_{i=1}^N$, where $f_i \in \mathbb{R}^{W \times H}$ denotes the feature map of the i -th input image, $c_i \in [1 : C]$ is the class label of the i -th input image, and W/H are the spatial sizes of the maps.

Method. We first partition \mathcal{F} as \mathcal{F}^c and \mathcal{F}^{-c} where $\mathcal{F}^c = \{f_i \mid (f_i, c_i) \in \mathcal{F}, c_i = c\}$ and $\mathcal{F}^{-c} = \{f_i \mid (f_i, c_i) \in \mathcal{F}, c_i \neq c\}$, $\forall c \in [1 : C]$. By this partition, we can find the corresponding statistics of \mathcal{F} in a two-class manner. Note each f_i in \mathcal{F}^c is a 2D feature map with $W \times H$ activations, and thus there are $|\mathcal{F}^c| \times W \times H$ activations in \mathcal{F}^c in total. We then define two statistics operators g_{mean} and g_{var} on \mathcal{F}^c , which return the mean and variance over these $|\mathcal{F}^c| \times W \times H$ activations. We can thus obtain the statistics $\mu_c = g_{mean}(\mathcal{F}^c)$ and $\sigma_c^2 = g_{var}(\mathcal{F}^c)$ for \mathcal{F}^c . The counterparts of \mathcal{F}^{-c} , μ_{-c} and σ_{-c}^2 , can be computed in the same way. The SD score for the two-class partition, $(\mathcal{F}^c, \mathcal{F}^{-c})$, can thus be derived as:

$$\text{SD}(\mathcal{F}^c, \mathcal{F}^{-c}) = \frac{1}{2} \left(\frac{\sigma_c^2}{\sigma_{-c}^2} + \frac{\sigma_{-c}^2}{\sigma_c^2} \right) + \frac{1}{2} \left(\frac{(\mu_c - \mu_{-c})^2}{\sigma_c^2 + \sigma_{-c}^2} \right) - 1 \quad (7)$$

$\text{SD}(\mathcal{F}^c, \mathcal{F}^{-c})$ captures the discriminativeness of class c relative to the other classes in \mathcal{F} . In general, we want to select channels that distinguish all classes well on average. Thus, under the C -class setting, the generalized Symmetric Divergence (G-SD) of \mathcal{F} is formally defined as:

$$\text{G-SD}(\mathcal{F}) = \frac{1}{C} \sum_{c=1}^C \text{SD}(\mathcal{F}^c, \mathcal{F}^{-c}) \quad (8)$$

7.3 High-Dimensional Metrics

We present the implementation of Discriminant Information (DI) [27] and Maximum Mean Discrepancy (MMD) [11] here. We use the same notation as in Section 7.2 and regard f_i as a flattened 1D vector.

DI. We first define two scatter matrices, $\bar{\mathbf{S}}$ and \mathbf{S}_B :

$$\bar{\mathbf{S}} = \sum_{i=1}^N (f_i - \bar{f})(f_i - \bar{f})^T \quad (9)$$

$$\mathbf{S}_B = \sum_{c=1}^C |\mathcal{F}^c| (\bar{f}^c - \bar{f})(\bar{f}^c - \bar{f})^T \quad (10)$$

where $\bar{f} = \frac{1}{N} \sum_{i=1}^N f_i$ and $\bar{f}^c = \frac{1}{N_c} \sum_{i=1}^{N_c} f_i$ represents the centroids of the all data and class c ($c \in [1 : C]$), respectively. DI is then defined as:

$$\text{DI}(\mathcal{F}) = \text{tr}([\bar{\mathbf{S}} + \rho \mathbf{I}]^{-1} \mathbf{S}_B) \quad (11)$$

where ρ is a small ridge factor to ensure invertibility. In practice, we set $\rho = 0.0001$.

MMD. We define the rbf kernel as:

$$k(x, y) = \exp\left\{-\frac{\|x - y\|_2^2}{2\sigma^2}\right\} \quad (12)$$

The two-class MMD on a $(\mathcal{F}^c, \mathcal{F}^{-c})$ partition can thus be defined as:

$$\begin{aligned} \text{MMD}_{two}(\mathcal{F}^c, \mathcal{F}^{-c}) &= \frac{1}{|\mathcal{F}^c|^2} \sum_{f_i, f_j \in \mathcal{F}^c} k(f_i, f_j) + \frac{1}{|\mathcal{F}^{-c}|^2} \sum_{f_i, f_j \in \mathcal{F}^{-c}} k(f_i, f_j) \\ &\quad - \frac{2}{|\mathcal{F}^c| \times |\mathcal{F}^{-c}|} \sum_{f_i \in \mathcal{F}^c, f_j \in \mathcal{F}^{-c}} k(f_i, f_j) \end{aligned} \quad (13)$$

following the similar one-versus rest setting, the MMD score of a channel can be defined as:

$$\text{MMD}(\mathcal{F}) = \frac{1}{C} \sum_{c=1}^C \text{MMD}_{two}(\mathcal{F}^c, \mathcal{F}^{-c}) \quad (14)$$

In practice, we set $\sigma = 1$ for the rbf kernel.

8 Pruned Models Details

We show the detailed structures of our pruned VGG-16 and ResNet-50 on ILSVRC-2012 in Table 3 and Table 4. Both pruned models are named as G-SD-B in the experimental results section. On VGG-16, we find that our algorithm prunes more channels in shallow layers, which indicates the shallow layers are less sensitive to pruning compared to the deep ones under the same overall FLOPs reduction. On ResNet-50, our model preserves more channels at the starting blocks of each stage. These blocks are the ones where the stride-2 downsamplings happen, which means that preserving information for the process of resolution reduction would be crucial to maintain the network's performance.

9 Time Complexity

We conduct an empirical study to investigate the time complexity of two discriminant functions, G-SD and DI, for channel scoring. We pick 3,000 ILSVRC-2012 samples and compute their feature maps in VGG-16. The maps are computed via an NVIDIA Tesla P100 GPU and the scorings of feature maps are executed on an Intel Xeon E5-2680 v4 CPU. We calculate the CPU wall time for scoring all the channels in each layer by the two discriminant functions (excluding the time to obtain the maps). From Fig. 6, we note that G-SD generally has much less time complexity than DI for each layer's channel scoring process. Moreover, for layer conv1_1 where the feature maps are of size 224×224 , G-SD shows a $4000 \times$ speedup over DI.

10 More Visualizations

We repeat the analysis in Section 5.1 with additional images from different classes (not shown in the main paper). Visually speaking, we again observe that our G-SD selects more class-discriminative channels compared to state-of-the-art metrics.

Layers	Parameters	FLOPs	Parameters (Pruned %)	FLOPs (Pruned %)
Original VGG-16		G-SD-B VGG-16		
conv1_1	1.7K	87M	0.3K (82.8)	14.9M (82.8)
conv1_2	36.9K	1.85B	3.9K (89.5)	0.19B (89.5)
conv2_1	73.7K	0.92B	21.1K (71.4)	0.26B (71.4)
conv2_2	0.15M	1.85B	49.7K (66.3)	0.62B (66.3)
conv3_1	0.29M	0.92B	92.7K (68.6)	0.29B (68.6)
conv3_2	0.59M	1.85B	97.8K (83.4)	0.31B (83.4)
conv3_3	0.59M	1.85B	0.17M (71.7)	0.52B (71.7)
conv4_1	1.18M	0.92B	0.43M (63.7)	0.34B (63.7)
conv4_2	2.36M	1.85B	0.52M (77.9)	0.41B (77.9)
conv4_3	2.36M	1.85B	0.67M (71.6)	0.53B (71.6)
conv5_1	2.36M	0.46B	1.47M (37.5)	0.29B (37.5)
conv5_2	2.36M	0.46B	2.02M (14.5)	0.40B (14.5)
conv5_3	2.36M	0.46B	2.02M (14.4)	0.40B (14.4)
fc_1	102.8M	0.10B	102.8M (0)	0.10B (0)
fc_2	16.8M	16.8M	16.8M (0)	16.8M (0)
fc_3	4.1M	4.1M	4.1M (0)	4.1M (0)
Total	138.34M	15.47B	131.19M (5.2)	4.68B (69.7)

Table 3: Detailed structure of the reported VGG-16 pruned model, G-SD-B (Top1-Accuracy: 71.26%). Fully connected layers are not pruned as 99.3% of the FLOPs are in the convolutional layers, which makes FLOPs pruning of fully connected layers less cost-effective.

Blocks	Parameters	FLOPs	Parameters (Pruned %)	FLOPs (Pruned %)
Original ResNet-50		G-SD-B ResNet-50		
Conv1	9.4K	0.12B	9.4K (0)	0.12B (0)
ResBlock1_1	73.7K	0.23B	42.5K (42.3)	0.13B (42.3)
ResBlock1_2	69.6K	0.22B	10.9K (84.3)	34.3M (84.3)
ResBlock1_3	69.6K	0.22B	25.5K (63.3)	80.1M (63.3)
ResBlock2_1	0.38M	0.37B	0.30M (20.8)	0.28B (25.2)
ResBlock2_2	0.28M	0.22B	49.9K (82.1)	39.1M (82.1)
ResBlock2_3	0.28M	0.22B	63.8K (77.1)	50.0M (77.1)
ResBlock2_4	0.28M	0.22B	93.0K (66.6)	72.9M (66.6)
ResBlock3_1	1.51M	0.37B	1.38M (8.7)	0.33B (10.6)
ResBlock3_2	1.11M	0.22B	0.38M (65.7)	74.9M (65.7)
ResBlock3_3	1.11M	0.22B	0.31M (72.2)	60.8M (72.2)
ResBlock3_4	1.11M	0.22B	0.30M (73.2)	58.6M (73.2)
ResBlock3_5	1.11M	0.22B	0.43M (61.4)	84.2M (61.4)
ResBlock3_6	1.11M	0.22B	0.69M (38.0)	0.14B (38.0)
ResBlock4_1	6.03M	0.37B	5.78M (4.2)	0.36B (4.3)
ResBlock4_2	4.46M	0.22B	3.72M (16.5)	0.18B (16.5)
ResBlock4_3	4.46M	0.22B	3.96M (11.1)	0.19B (11.1)
fc1	2.05M	2.05M	2.05M (0)	2.05M (0)
Total	25.50M	4.09B	19.59M (23.2)	2.28B (44.3)

Table 4: Detailed structure of the reported ResNet-50 pruned model, G-SD-B (Top1-Accuracy: 75.85%). We choose not to prune Conv1 and fc1 for the ease of implementation.

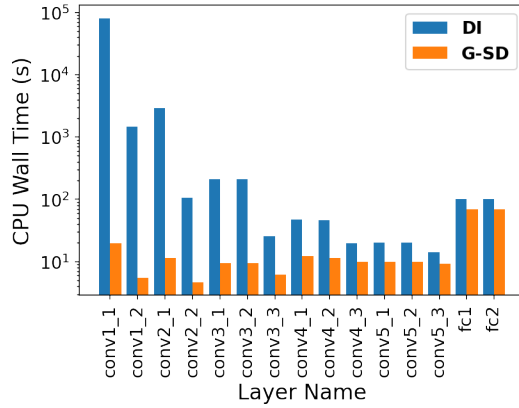


Figure 6: The CPU wall time for scoring all channels in VGG-16 layers by G-SD and DI on ILSVRC-2012.

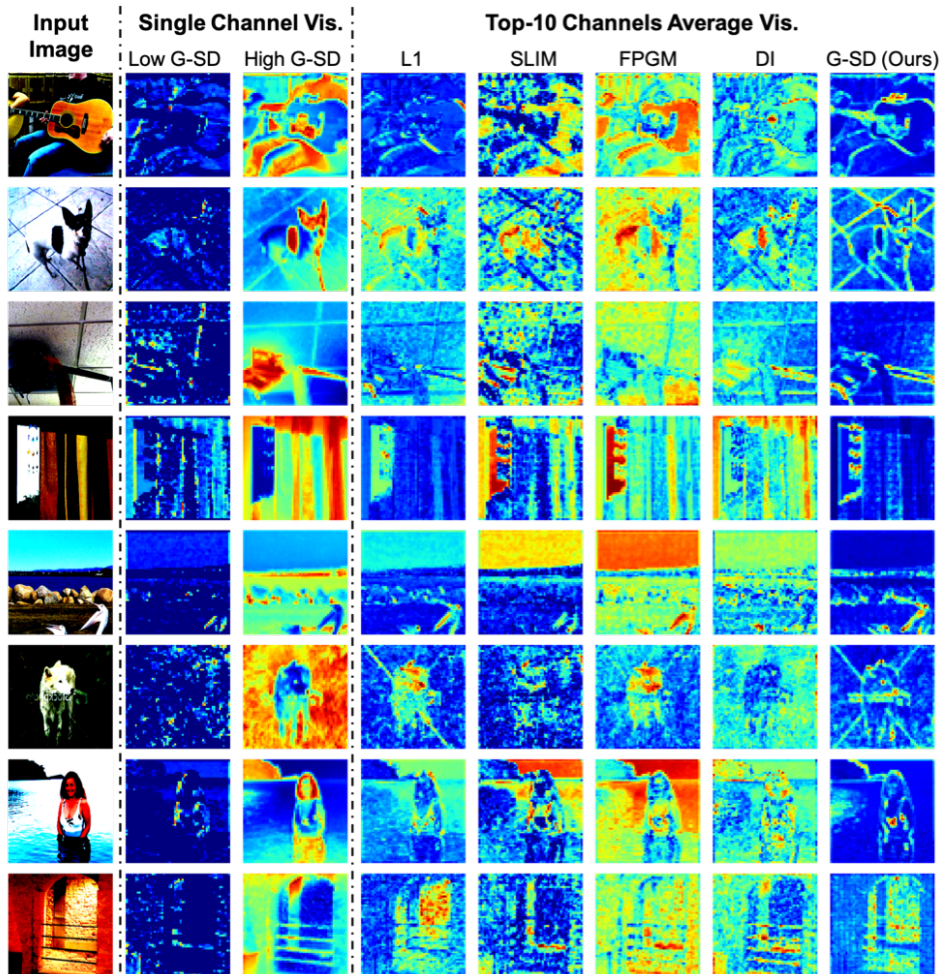


Figure 7: More visualizations of the qualitative channel selection analysis. **Col. 1:** Input images. **Col. 2-3:** Single channel visualization on channels with low and high G-SD values. **Col. 4-8:** Average responses of the top-10 channels selected by different metrics. From left to right, the metrics are: ℓ_1 -norm [33], batch-norm scaling factor [37], filter’s geometric median [20], DI [27], and G-SD.